Photosynthesis Research
https://doi.org/10.1007/s11120-023-01051-9

RESEARCH

Mn-porphyrins in a four-helix bundle participate in photo-induced electron transfer with a bacterial reaction center

J. C. Williams[1] · M. S. Faillace[1] · E. J. Gonzalez[1] · R. E. Dominguez[1] · K. Knappenberger[1] · D. A. Heredia[1] · T. A. Moore[1] · A. L. Moore[1] · J. P. Allen[1]

Received: 21 July 2023 / Accepted: 18 September 2023

Abstract

Hybrid complexes incorporating synthetic Mn-porphyrins into an artificial four-helix bundle domain of bacterial reaction centers created a system to investigate new electron transfer pathways. The reactions were initiated by illumination of the bacterial reaction centers, whose primary photochemistry involves electron transfer from the bacteriochlorophyll dimer through a series of electron acceptors to the quinone electron acceptors. Porphyrins with diphenyl, dimesityl, or fluorinated substituents were synthesized containing either Mn or Zn. Electrochemical measurements revealed potentials for Mn(III)/Mn(II) transitions that are ~ 0.4 V higher for the fluorinated Mn-porphyrins than the diphenyl and dimesityl Mn-porphyrins. The synthetic porphyrins were introduced into the proteins by binding to a four-helix bundle domain that was genetically fused to the reaction center. Light excitation of the bacteriochlorophyll dimer of the reaction center resulted in new derivative signals, in the 400 to 450 nm region of light-minus-dark spectra, that are consistent with oxidation of the fluorinated Mn(II) porphyrins and reduction of the diphenyl and dimesityl Mn(III) porphyrins. These features recovered in the dark and were not observed in the Zn(II) porphyrins. The amplitudes of the signals were dependent upon the oxidation/reduction midpoint potentials of the bacteriochlorophyll dimer. These results are interpreted as photo-induced charge-separation processes resulting in redox changes of the Mn-porphyrins, demonstrating the utility of the hybrid artificial reaction center system to establish design guidelines for novel electron transfer reactions.

Keywords Photosynthesis · Electron transfer · Protein design

Abbreviations

P	Bacteriochlorophyll dimer of reaction centers
Q_A	Primary quinone electron acceptor of reaction centers
Q_B	Secondary quinone electron acceptor of reaction centers
PB1	Single-chain four-helix bundle protein
LH(L131) + LH(M160) + FH(M197)	High-potential reaction center containing the alterations L131 Leu to His, M160 Leu to His, and M197 Phe to His

✉ J. P. Allen
jallen@asu.edu

[1] School of Molecular Sciences, Arizona State University, Tempe, AZ 85287, USA

Published online: 01 November 2023

MPB2	High-potential reaction center and four-helix bundle fusion protein
Mn(III) $(CF_3)_2(pheF_5)_2$porphyrin	Mn(III) 5,15-bis(perfluorophenyl)-10,20--bis(trifluoromethyl) porphyrin
Zn(II) $(CF_3)_2(pheF_5)_2$porphyrin	Zn(II) 5,15-bis(perfluorophenyl)-10,20--bis(trifluoromethyl) porphyrin
Mn(III) $(CF_3)_4$porphyrin	Mn(III) 5,10,15,20-tetrakis-(trifluoromethyl)porphyrin
Zn(II) $(CF_3)_4$porphyrin	Zn(II) 5,10,15,20-tetrakis-(trifluoromethyl)porphyrin
Mn(III) $(phe)_2$porphyrin	Mn(III) 5,15-diphenylporphyrin
Zn(II) $(phe)_2$porphyrin	Zn(II) 5,15-diphenylporphyrin
Mn(III) $(mes)_2$porphyrin	Mn(III) 5,15-dimesitylporphyrin
Zn(II) $(mes)_2$porphyrin	Zn(II) 5,15-dimesitylporphyrin

Introduction

The controlled flow of electrons in cells is crucial for many key biological reactions, including photosynthesis and respiration. Replication of these processes in artificial complexes provides both an understanding of the natural systems and a platform for studying novel reactions. Towards this end, the convergence of progress in the design of de novo proteins, synthetic constructs, and modifications of existing proteins presents an opportunity for the creation of hybrid artificial photosynthetic reaction centers. Each of these elements contributes to the goal of achieving a new electron transfer pathway that is well-defined, reversible, and triggered using light.

The four-helix bundle is a workhorse in the field of protein design. Four-helix bundles are capable of binding a wide range of cofactors, including metal clusters and porphyrins (Farid et al. 2013; Lu et al. 2018; Lombardi et al. 2019). The robust configuration is stable under a variety of conditions including either aqueous or membrane environments, and the polypeptide is easily expressed and isolated. In the de novo design of a photosynthetic complex, Dutton and coworkers have demonstrated the utility of four-helix bundles for tightly binding porphyrins and for combining multiple components that are found as cofactors in photosystems, such as porphyrins, metal clusters, and tyrosine residues (Ennist et al. 2022). While the addition of external oxidants and reductants can change the redox states of bound cofactors, currently the field has had limited success in achieving efficient and reversible chemical reactions by redox-active cofactors.

Porphyrins are versatile photoactive compounds and cofactors in proteins. Control of their characteristic spectra, photoelectrochemical, and redox properties can be achieved by judicious substitution of metalloporphyrins. The redox properties extend over a wide range, depending on the choice of the central metal and substituents. Biological electron and proton-transfer processes can be reproduced with these synthetic systems. Molecular dyads and triads incorporating porphyrins have been used as mimics of photosynthesis, and can also include analogs of the side chains of amino acids such as histidine and tyrosine (Mora et al. 2018; Yoneda et al. 2021; Arsenault et al. 2022). Incorporation of such constructs into artificial proteins extends the range of these bioinspired systems by the addition of interactions with the polypeptide side chains or other bound cofactors. For four-helix bundles, the molecules can be encased in a hydrophobic interior with a hydrophilic exterior, allowing manipulation in aqueous solutions and the ability to dock with biological proteins. In particular, artificial proteins provide a bridge between synthetic porphyrins and biological photosynthetic proteins to enable participation in energy and electron transfer.

Among the photosynthetic proteins, bacterial reaction centers have proven useful for probing the factors that control electron transfer in large biological complexes (Williams and Allen 2009). In reaction centers, after light is absorbed by the bacteriochlorophyll dimer, P, an electron is transferred through one of the branches of cofactors to the primary quinone, Q_A, followed by transfer to the secondary quinone, Q_B (Woodbury and Allen 1995; Niedringhaus et al. 2018). Accompanying the transfer of a second electron is the uptake of two protons, with the resulting quinol released into the membrane and replaced with an exogenous quinone (Okamura et al. 2000; Wraight 2006). On the donor side, the oxidized bacteriochlorophyll dimer can be reduced by a number of secondary electron donors in addition to the native cytochrome c_2. For example, by using mutations to adjust the redox potential of the dimer and to create binding sites, transition metals such as Mn can reduce the oxidized dimer (Espiritu et al. 2020).

Hybrid complexes with protein domains having novel molecules as bound cofactors have been employed as a strategy for producing functional proteins that recognize molecular features or are capable of performing energy transfer (Mancini et al. 2017; Grayson et al. 2017; Liu et al. 2020; Yang et al. 2021). In previous work, we have shown that Mn or protoporphyrin IX cofactors bound to de novo proteins can dock on the periplasmic surface of the reaction center and reduce the oxidized bacteriochlorophyll dimer, P^+ (Olson et al. 2016, 2017; Espiritu et al. 2020;

Allen et al. 2022). In this study, we utilize a hybrid fusion framework with a de novo protein genetically fused to the reaction center to investigate the potential for new electron transfer reactions. MPB2 is a reaction center that has been modified to contain a domain consisting of a single-chain four-helix bundle fused to the C-terminus of the M subunit as described previously (Calhoun et al. 2003; Allen et al. 2022). In addition, the reaction centers are highly oxidizing due to the alterations of L131 Leu to His, M160 Leu to His, and M197 Phe to His (Lin et al. 1994a). These reaction centers have the ability to perform light-induced electron transfer from the excited state of P to Q_A but also possess the additional feature of a porphyrin near P that could participate in electron transfer with P (Fig. 1). Our model is based on one porphyrin bound to the four-helix bundle of the fusion reaction center. The available structural information shows that one porphyrin will bind to four-helix bundles of this size (Mann et al. 2021; Ennist et al. 2022). In addition, we have previously shown that protoporphyrin IX does not interact with the reaction centers in the absence of the four-helix bundle (Allen et al. 2022).

By using reaction centers as a base in a hybrid complex, novel redox reactions involving synthetic porphyrins can be initiated using light excitation of the bacteriochlorophyll dimer. Key to the placement of synthetic porphyrins in the hybrid reaction centers is the design, synthesis, and characterization of porphyrins with specific properties. Computer modeling was used to screen for the viability of binding porphyrins to the four-helix bundle of the fusion protein.

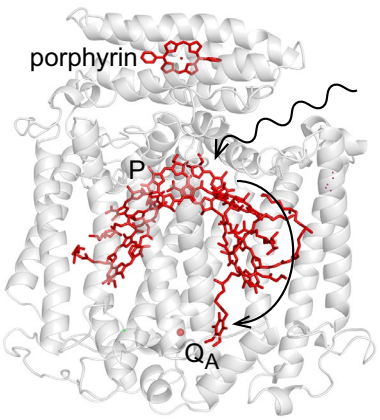

Fig. 1 Model of the MPB2 hybrid reaction center, based on the fusion of a four-helix bundle to the reaction center through the C-terminus of the M subunit, with binding of a porphyrin to the four-helix bundle. In the reaction center portion, absorption of light results in excitation of the bacteriochlorophyll dimer, P, and subsequent electron transfer through the cofactors (red) to the primary electron acceptor, Q_A, as shown by the curved arrow. The presumed placement of the four-helix bundle generated by this computer model shows the position of the porphyrin near P. For clarity, only the L and M subunits (light gray) are displayed

Modeling showed that porphyrins with a variety of substituents could be placed into the four-helix bundle with proper coordination from His ligands without steric hindrance. With this position, the porphyrin location is comparable to those identified in X-ray structures of porphyrin-containing bundles (Mann et al. 2021; Ennist et al. 2022). This placement of synthetic porphyrins in the hybrid reaction centers provides the opportunity to investigate novel electron transfer processes. Specifically, we tested eight different metalloporphyrins containing either Mn or Zn. Four of the porphyrins had fluorinated substituents and were compared to the nonfluorinated counterparts (Fig. 2). Optical spectroscopy and redox measurements were used to examine the properties of the synthetic porphyrins. The porphyrins in the hybrid reaction centers were characterized by optical spectroscopy to examine their participation in light-induced electron transfer.

Materials and methods

Preparation of porphyrins, four-helix bundle, reaction centers, and fusion proteins

Eight metalloporphyrins were synthesized (Fig. 2). Four porphyrins had fluorinated substituents: Mn(III) 5,15-bis(perfluorophenyl)-10,20-bis(trifluoromethyl)porphyrin (Mn(III) $(CF_3)_2(pheF_5)_2$porphyrin), Mn(III) 5,10,15,20-tetrakis(trifluoromethyl)porphyrin (Mn(III) $(CF_3)_4$porphyrin), Zn(II) 5,15-bis(perfluorophenyl)-10,20-bis(trifluoromethyl)porphyrin (Zn(II) $(CF_3)_2$-$(pheF_5)_2$porphyrin), and Zn(II) 5,10,15,20-tetrakis(trifluoromethyl)porphyrin (Zn(II) $(CF_3)_4$porphyrin). These were compared to four nonfluorinated porphyrins: Mn(III) 5,15-diphenylporphyrin (Mn(III) $(phe)_2$porphyrin), Mn(III) 5,15-dimesitylporphyrin (Mn(III) $(mes)_2$porphyrin), Zn(II) 5,15-diphenylporphyrin (Zn(II) $(phe)_2$porphyrin), and Zn(II) 5,15-dimesitylporphyrin (Zn(II) $(mes)_2$porphyrin). The Supplementary Information contains a detailed description of the preparation of these eight porphyrins. Briefly, the *meso*-free and *meso*-CF_3 substituted dipyrromethanes were synthesized by standard procedures, and the porphyrins were prepared by condensation of the dipyrromethanes with the corresponding aldehydes or direct condensation of pyrrol-alcohol (Wijesekera 1996; Shimizu et al. 2006). The free base porphyrins were metalated following published procedures (Chizhova et al. 2018).

The single-chain four-helix bundle, PB1, is a water-soluble protein with a His tag for purification (Calhoun et al. 2003; Allen et al. 2022). The MPB2 reaction centers contain a single-chain four-helix bundle fused to the C-terminus of the M subunit as described previously (Allen et al. 2022). The C-terminal residue of the M subunit, which is located

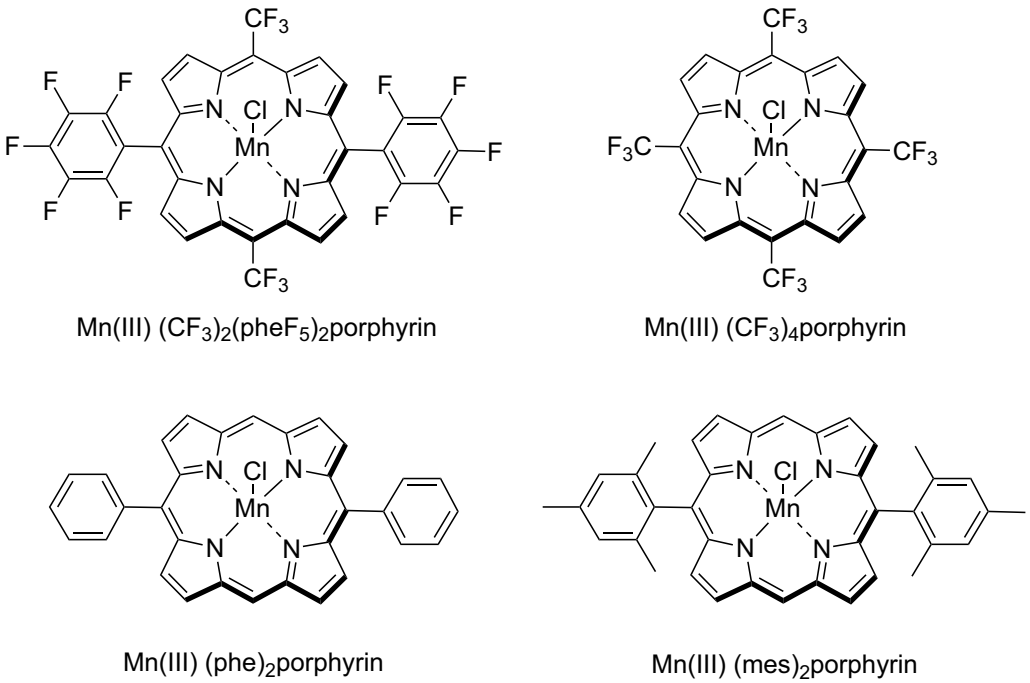

Fig. 2 Chemical structures of the four synthetic Mn-porphyrins, Mn(III) $(CF_3)_2(pheF_5)_2$porphyrin, Mn(III) $(CF_3)_4$porphyrin, Mn(III) $(phe)_2$porphyrin and Mn(III) $(mes)_2$porphyrin

shortly after the transmembrane helix E, is connected to the four-helix bundle with a Gly linker that has the sequence GGNGGN. After the C-terminal residue of the four-helix bundle is a cleavable His tag for purification. Reaction centers containing mutations that alter the P^+/P midpoint potential have been described previously (Lin et al. 1994a). The region surrounding P in the MPB2 reaction center contains three mutations, L131 Leu to His, M160 Leu to His, and M197 Phe to His, that raise the P^+/P midpoint potential to 0.76 V vs. SHE (Lin et al. 1994a). The genes for the PB1 protein and MPB2 fusion protein were expressed in *Escherichia coli* and *Rhodobacter sphaeroides*, respectively (Fig. S40). The construction of the genes has been described previously (Allen et al. 2022). The PB1 protein was purified by affinity chromatography, and the His tag was removed by protease cleavage. Reaction centers were isolated using the detergent lauryl dimethylamine oxide to solubilize the protein from the cell membrane, purified using affinity or ion exchange chromatography, and then concentrated and exchanged into the appropriate buffer, generally 15 mM CHES pH 9.4 and 0.05% Triton X-100. To block electron transfer from Q_A to Q_B, 100 µM terbutryn was added.

Binding of porphyrins to four-helix bundle protein and fusion reaction centers

The porphyrins were dissolved in dimethyl sulfoxide at 1 mM concentrations prior to addition to the proteins. The Mn-porphyrins were bound to the PB1 four-helix bundle by incubating 20 µM porphyrin with 10 µM PB1 protein in 15 mM CHES pH 9.4 for 0.5 to 1 h by rocking at room temperature. In some cases, the sample was washed by sequentially diluting and concentrating the sample using a 3000 Da centrifugal filter (Amicon), followed by dilution into 15 mM CHES pH 9.4. For the MPB2 fusion reaction centers, measurements were performed on samples where the porphyrins were added by incubating 2 µM reaction centers with 6 µM Mn-porphyrin or 1 µM Zn–porphyrin for at least 30 min at room temperature in 15 mM CHES pH 9.4, 0.05% Triton X-100, and 100 µM terbutryn. For measurements with the wild-type reaction centers and reaction centers with altered P^+/P midpoint potentials, samples contained 2 µM reaction centers and 10 µM Mn-porphyrin bound to the PB1 four-helix bundle in 15 mM CHES pH 9.4, 0.05% Triton X-100, and 100 µM terbutryn.

Spectroscopy

Optical measurements were performed using a Varian Cary 6000i spectrophotometer, with illumination from an Oriel lamp through an 860 nm interference filter. Light-minus-dark spectra were taken using a dark baseline, and light-induced absorption changes were identified during a 90-s sweep from 1000 to 350 nm or a 60-s sweep from 650 to 350 nm during illumination. Subsequent difference spectra were measured in the dark. The kinetics of the absorption changes at specific wavelengths were measured using 90-s illumination, except where indicated otherwise.

Results

Redox states of the Mn-porphyrins and Zn-porphyrins

Four Mn-porphyrins were studied, Mn(III) $(CF_3)_2(pheF_5)_2$porphyrin, Mn(III) $(CF_3)_4$porphyrin, Mn(III) $(phe)_2$porphyrin, and Mn(III) $(mes)_2$porphyrin (Fig. 2 and Supplementary Information). The absorption spectrum of the Mn(III) $(CF_3)_2(pheF_5)_2$porphyrin in dichloromethane has major peaks at 332 nm and 349 nm, with smaller peaks at 420, 469, 569 and 610 nm; while the Mn(III) $(CF_3)_4$porphyrin spectrum has major peaks at 348, 420 and 464 nm and smaller peaks at 572, and 616 (Fig. S27, S29). The absorption spectra of the Mn(III) $(phe)_2$porphyrin and Mn(III) $(mes)_2$porphyrin in dichloromethane have a major peak at 470 nm, with smaller peaks at 367, 395, 515, 569, and 601 nm and a weak band near 752 nm, consistent with a Mn(III) state (Figs. S8B, S10B).

Using cyclic voltammetry, the Mn-porphyrins in dichloromethane were found to be redox active with $E_{1/2}$(Mn(III)/Mn(II)) values of + 0.33, + 0.29, − 0.05, and − 0.09 V versus SHE for Mn(III) $(CF_3)_2(pheF_5)_2$porphyrin, Mn(III) $(CF_3)_4$porphyrin, Mn(III) $(phe)_2$porphyrin, and Mn(III) $(mes)_2$porphyrin, respectively (Figs. 3, S30–S39). No peaks were observed corresponding to an oxidation/reduction transition near 0 V in the corresponding Zn-porphyrins. For all porphyrins, additional peaks were evident that are assigned to the porphyrin ring and not to a change of the redox state of the metal (Harriman et al. 1979; Porhiel et al. 2000; Lin et al. 2002).

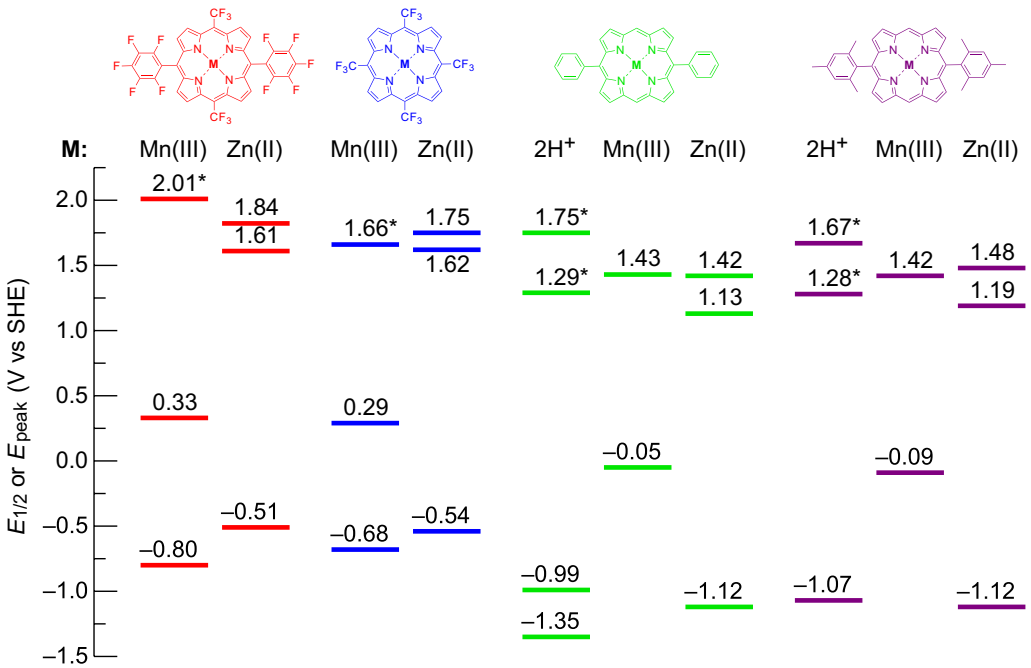

Fig. 3 Summary of the electrochemical properties of the synthetic porphyrins. Values are shown for Mn(III) $(CF_3)_2(pheF_5)_2$porphyrin and Zn(II) $(CF_3)_2(pheF_5)_2$porphyrin (red), Mn(III) $(CF_3)_4$porphyrin and Zn(II) $(CF_3)_4$porphyrin (blue), Mn(III) $(phe)_2$porphyrin and Zn(II) $(phe)_2$porphyrin as well as the free base porphyrin (green), and Mn(III) $(mes)_2$porphyrin and Zn(II) $(mes)_2$porphyrin as well as the free base porphyrin (purple). These values were determined from the cyclic voltammograms of the individual porphyrins (Figs. S30–S39). All the potentials are $E_{1/2}$, unless E_{peak} is indicated, for irreversible processes (*). Although only the first oxidation and reduction potentials are important for this work, the $E_{1/2}$ and E_{peak} are included for the waves observed at higher and lower potentials to more completely characterize the electrochemistry of these porphyrins

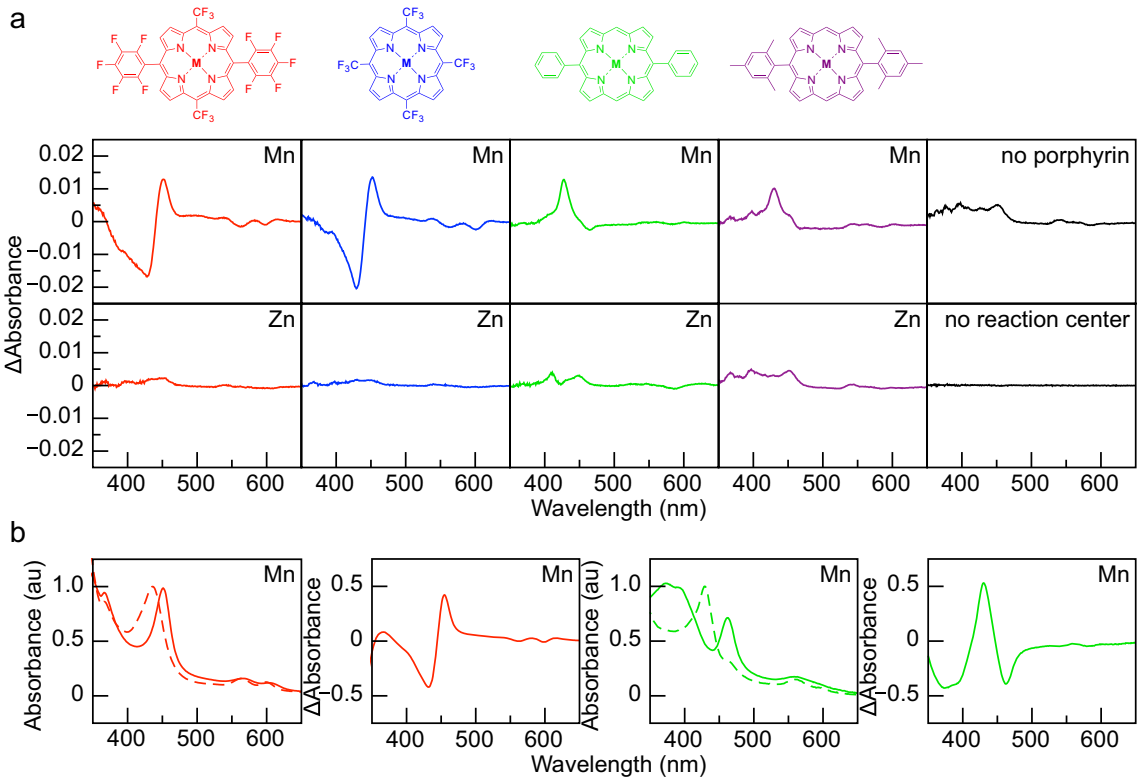

Fig. 4 Spectra of MPB2 fusion reaction centers and PB1 four-helix bundle with different porphyrins. **a** Light-minus-dark absorption spectra of MPB2 fusion reaction centers with Mn(II) $(CF_3)_2(pheF_5)_2$porphyrin and Zn(II) $(CF_3)_2(pheF_5)_2$porphyrin (red), Mn(II) $(CF_3)_4$porphyrin and Zn(II) $(CF_3)_4$porphyrin (blue), Mn(III) $(phe)_2$porphyrin and Zn(II) $(phe)_2$porphyrin (green), and Mn(III) $(mes)_2$porphyrin and Zn(II) $(mes)_2$porphyrin (purple), as well as no porphyrin and the PB1 four-helix bundle with Mn(III) $(phe)_2$porphyrin but no reaction center (black). The signals show a red-shift consistent with oxidation of Mn(II) $(CF_3)_2(pheF_5)_2$porphyrin and Mn(II) $(CF_3)_4$porphyrin and a blue-shift consistent with reduction of Mn(III) $(phe)_2$porphyrin and Mn(III) $(mes)_2$porphyrin in the light, but no significant differences for the Zn(II) porphyrins compared to reaction centers without porphyrin, and no change in the porphyrin in the four-helix bundle with no reaction center upon exposure to illumination at 860 nm. **b** Absorption spectra of the four-helix bundle PB1 with Mn(III) $(CF_3)_2(pheF_5)_2$porphyrin in PB1 (solid red) and Mn(III) $(phe)_2$porphyrin (solid green). The spectra shift upon addition of 0.4 mM sodium dithionite (dashed red) and 0.6 mM sodium dithionite (dashed green). Subtraction of these spectra results in a calculated oxidized-minus-reduced difference spectrum (second panel) and reduced-minus-oxidized difference spectrum (fourth panel)

Porphyrin binding to four-helix bundles and fusion reaction centers

The initial screening for binding of the Mn-porphyrins was done using the purified single-chain four-helix bundle protein designated PB1 to avoid the spectral congestion of reaction centers (Fig. 4). The optical spectrum of the PB1 four-helix bundle with bound Mn(III) $(CF_3)_2(pheF_5)_2$porphyrin showed a major peak at 451 nm, and minor peaks at 367, 567, and 605 nm. The PB1 four-helix bundle with bound Mn(III) $(phe)_2$porphyrin had a major peak at 460 nm, and minor peaks at 375, 390, and 560 nm. Upon the addition of sodium dithionite, the peaks of the Mn-porphyrins shifted, for example, the major peak of Mn(III) $(CF_3)_2(pheF_5)_2$porphyrin shifted from 451 to 430 nm, reflecting the reduction from Mn(III) to Mn(II). The other Mn-porphyrins showed similar shifts upon reduction. Thus, the distinctive spectra of the reduced and oxidized states of the Mn-porphyrins provided an optical signature for detecting a light-induced redox change when bound to reaction centers. After addition of either Mn(III) $(CF_3)_2(pheF_5)_2$porphyrin or Mn(III) $(CF_3)_4$porphyrin to solutions containing the PB1 protein or MPB2 reaction centers, a slow shift of the absorption peaks was observed over ~ 1 h in the dark, indicating reduction to the Mn(II) porphyrin redox state.

For the electron transfer measurements, the porphyrins were bound to the fusion reaction centers designated MPB2 that contain a four-helix bundle domain linked to the C-terminus of the M subunit of the reaction center. The porphyrin binding to the MPB2 fusion reaction center followed similar procedures to the four-helix bundle alone, with the addition of a detergent to

keep the reaction centers in solution. The absorption spectra of the fusion reaction centers after the addition of Mn-porphyrin showed the presence of new peaks (Fig. S41). For the fluorinated Mn-porphyrins, the peak at 430 nm is consistent with the reduced state, Mn(II) $(CF_3)_2(pheF_5)_2$porphyrin and Mn(II) $(CF_3)_4$porphyrin. The peak at 463 nm for Mn(III) $(phe)_2$porphyrin and Mn(III) $(mes)_2$porphyrin indicates the presence of the Mn(III) oxidization state. The addition of Zn-porphyrins to the fusion reaction centers resulted in new peaks in the MPB2 spectrum at 418 for the fluorinated Zn(II) porphyrins and 422 nm for Zn(II) $(phe)_2$porphyrin and Zn(II) $(mes)_2$porphyrin.

Light-induced redox changes of Mn-porphyrins bound to fusion reaction centers

Light-minus-dark spectra were measured to characterize the porphyrin redox changes upon light excitation of P in the MPB2 fusion reaction centers using continuous illumination through an 860 nm interference filter. After the baseline was recorded in the dark, light-minus-dark spectra were measured during a 90 s illumination, then the spectra were measured again in the dark at various times after illumination. In the presence of either Mn(II) $(CF_3)_2(pheF_5)_2$porphyrin or Mn(II) $(CF_3)_4$porphyrin bound to the MPB2 fusion reaction centers, a distinctive red-shift derivative signal was observed in the visible region, appearing as a loss of absorption at 430 nm and a positive peak at 450 nm, in the light-minus-dark spectra (Fig. 4). These spectra match the predicted optical signal for oxidation of the Mn(II) porphyrins to Mn(III) porphyrins. In contrast, a blue-shift derivative signal was observed for Mn(III) $(phe)_2$porphyrin or Mn(III) $(mes)_2$porphyrin bound to the MPB2 fusion reaction centers, having a peak near 430 nm and a minimum at 460 nm and matching the predicted optical signal for reduction of these Mn(III) porphyrins to Mn(II) porphyrins.

For the fusion reaction centers in the absence of Mn-porphyrin, a small broad absorption increase with minor peaks was observed in the visible region of the spectrum after illumination (Fig. 4). The small features are associated with the $P^+Q_A^-$ charge-separated state, which also has characteristic features in the near-infrared region arising from the oxidized dimer and reduced quinone (Fig. S42). The light-minus-dark spectra obtained after the addition of the four Zn(II) porphyrins were similar to those when no porphyrin was added. The excitation region centered at 860 nm does not overlap with any of the absorption bands of the porphyrins, and no significant spectral changes were observed after illumination of the Mn(III) $(phe)_2$porphyrin bound to the PB1 four-helix bundle in the absence of the reaction center (Fig. 4).

Kinetics of Mn-porphyrin redox change and recovery

The time dependences of the optical signals associated with redox changes of the Mn-porphyrins bound to the MPB2 fusion reaction centers were characterized by monitoring the 430 nm (or 427 nm) absorption signals (Fig. 5). For Mn(II) $(CF_3)_2(pheF_5)_2$porphyrin and Mn(II) $(CF_3)_4$porphyrin bound to MPB2 reaction centers, illumination resulted in a rapid decrease of the absorption at 430 nm that fully recovered in the dark. This change is associated with the oxidation of Mn(II) to Mn(III) vide infra. Light-induced absorption changes were compared at different wavelengths for Mn(II) $(CF_3)_2(pheF_5)_2$porphyrin bound to MPB2 reaction centers (Fig. 6). A loss of the reduced state of the Mn-porphyrin was observed by the

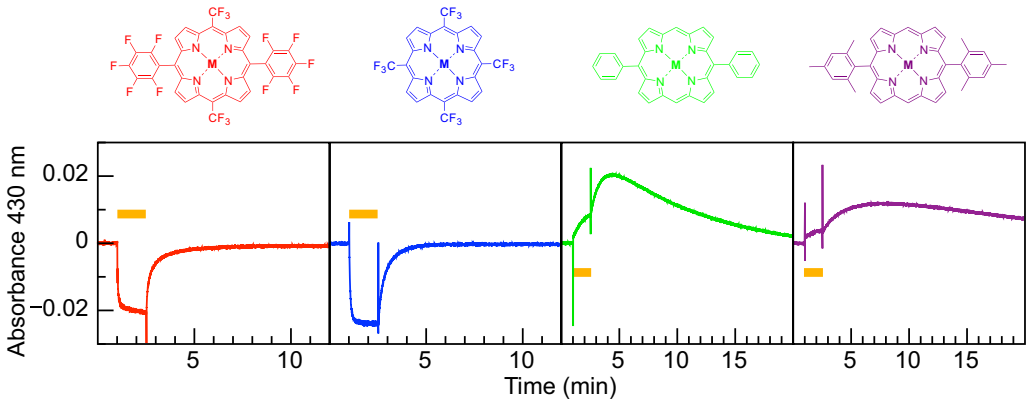

Fig. 5 Kinetics of light-induced changes of MPB2 fusion reaction centers containing Mn(II) $(CF_3)_2(pheF_5)_2$porphyrin (red), Mn(II) $(CF_3)_4$porphyrin (blue), Mn(III) $(phe)_2$porphyrin (green), and Mn(III) $(mes)_2$porphyrin (purple). The time dependence of the optical signal was measured at 430 nm, except for samples with Mn(III) $(phe)_2$porphyrin, which was measured at 427 nm. The decrease at 430 nm is attributed to oxidation of the Mn(II) porphyrins, while the increase corresponds to reduction of the Mn(III) porphyrins. The samples were illuminated at 860 nm for 90 s (orange bar)

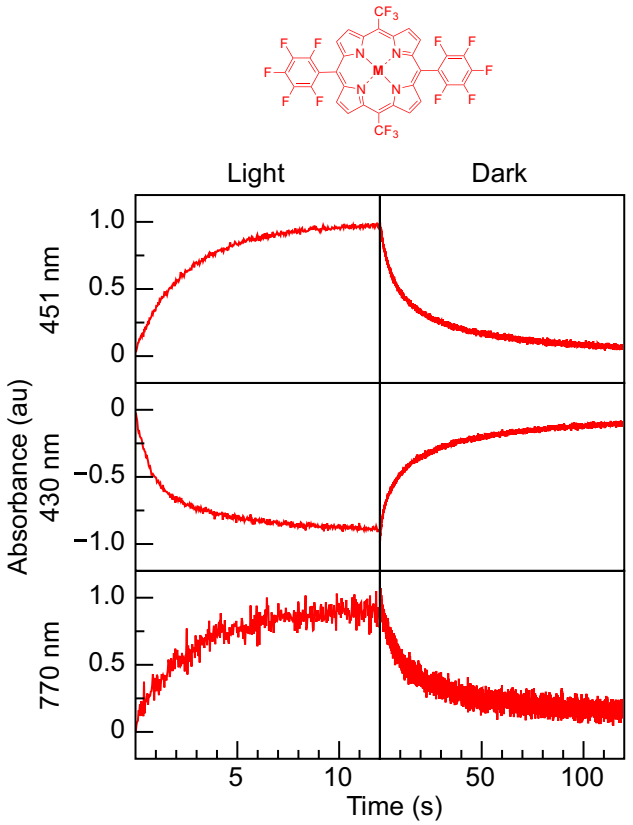

Fig. 6 Kinetics of light-induced changes in MPB2 fusion reaction centers with Mn(II) $(CF_3)_2(pheF_5)_2$porphyrin measured at three different wavelengths, 451, 430, and 770 nm, during illumination (left) and in the dark after illumination (right). The signals at each wavelength are normalized to the largest optical change during illumination. The samples were illuminated at 860 nm for 90 s

absorption decrease at 430 nm while a gain of the oxidized state was observed as an increase in absorption at 451 nm. The reduction of the primary quinone was evidenced by the increase in absorption at 770 nm, arising from an electrostatic interaction between the reduced quinone and active bacteriopheophytin monomer (Woodbury and Allen 1995; Niedringhaus et al. 2018). The kinetic data were fit with exponential terms (Fig. S43). The absorption changes in the light, representing the overall accumulation of the light-induced state, occurred with a time of approximately 2 s. For each wavelength, the absorption changes fully recovered in the dark. The decay time was approximately 10 s, although a second component with a time on the order of minutes was present. This longer component was also observed in MPB2 reaction centers with no porphyrin, and is typical of charge recombination after continuous illumination. Similar kinetics at these wavelengths were observed for Mn(II) $(CF_3)_4$porphyrin bound to MPB2 reaction centers.

In contrast, the MPB2 reaction centers with either Mn(III) $(phe)_2$porphyrin or Mn(III) $(mes)_2$porphyrin showed significantly different behaviors. During illumination, an initial increase in the absorption near 430 nm was followed by a slower increase. This change is associated with the reduction of Mn(III) to Mn(II) vide infra. When illumination was ended, the absorption continued to increase in the dark for up to a few minutes. After reaching a maximum, the signal decreased over several minutes for the sample with Mn(III) $(phe)_2$porphyrin bound to the MPB2 reaction centers. The signal decreased more slowly in the dark for samples with Mn(III) $(mes)_2$porphyrin bound to the MPB2 reaction centers.

Dependence of Mn-porphyrin redox reaction on the P^+/P midpoint potential

To investigate the influence of the P^+/P midpoint potential on the redox changes of the Mn-porphyrins, the absorption changes were measured for samples that contained the porphyrins bound to the PB1 four-helix bundle and added to reaction centers with no four-helix bundle fusion domain (Fig. 7). In these experiments the four-helix bundles with bound Mn-porphyrin were docked to the reaction centers. The samples contained either high-potential reaction centers, which have a P^+/P midpoint potential of 765 mV, or wild-type reaction centers, which have a P^+/P midpoint potential of 505 mV vs. SHE (Lin et al. 1994a). The high-potential LH(L131) + LH(M160) + FH(M197) reaction centers have the same three mutations near P as the MPB2 fusion reaction centers. For these reaction centers and reaction centers with intermediate P^+/P midpoint potentials, the amplitudes of spectral changes associated with the $P^+Q_A^-$ charge-separated state are inversely proportional to the P^+/P midpoint potential, as observed both in the kinetic measurements and the light-minus-dark spectra (Fig. S44), resulting from the previously described changes in quantum yield (Williams and Allen 2009).

The kinetics of the absorption changes at 453 nm measured for samples that contained the Mn(II) $(CF_3)_2(pheF_5)_2$porphyrin bound to the PB1 four-helix bundle and added to reaction centers with no four-helix domain were similar to those for the same porphyrin bound to the MPB2 fusion reaction centers (Fig. 7). For the high-potential reaction centers, absorption changes were observed that are significantly larger than those observed in the absence of the Mn-porphyrin. For wild-type reaction centers, the changes with the Mn-porphyrin were much smaller than those observed for the high-potential reaction centers, and were of similar amplitudes to the reaction centers without the Mn-porphyrin.

The samples with Mn(III) $(phe)_2$porphyrin bound to the four-helix bundle and added to high-potential reaction

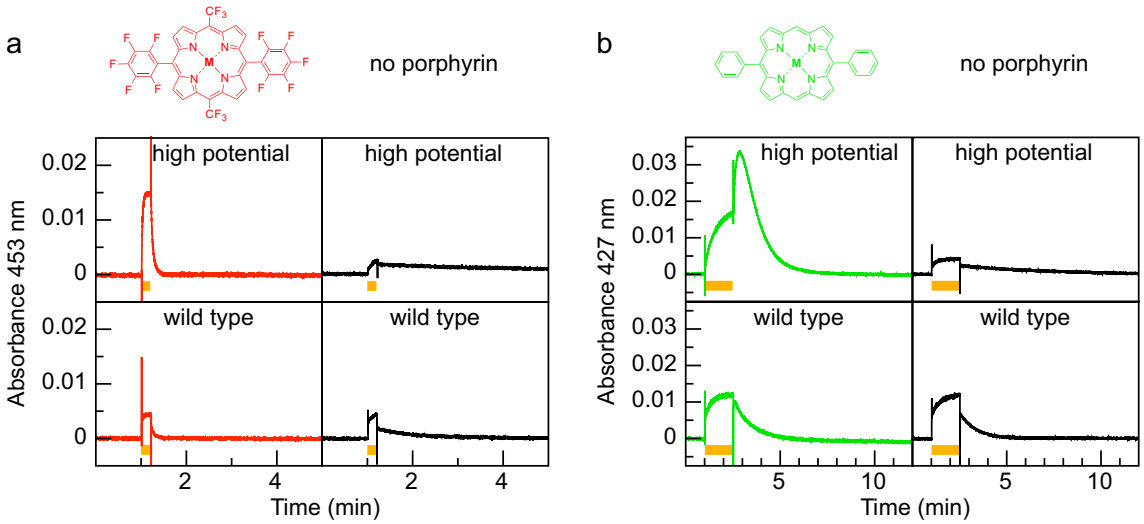

Fig. 7 Time dependences of the absorbance at 453 nm or 427 nm during and after illumination for samples with wild-type and high-potential LH(L131) + LH(M160) + FH(M197) reaction centers, having P^+/P midpoint potentials of 505 and 765 mV vs. SHE, respectively. The samples contained either reaction centers and the Mn-porphyrin bound to the PB1 four-helix bundle or reaction centers alone with no porphyrin **a** Absorbance changes at 453 nm for samples with reaction centers and Mn(II) $(CF_3)_2(pheF_5)_2$porphyrin bound to the PB1 four-helix bundle (red) compared to reaction centers only (black). The samples were illuminated at 860 nm for 12 s (orange bar). **b** Absorbance changes at 427 nm for samples containing reaction centers and Mn(III) $(phe)_2$porphyrin bound to the PB1 four-helix bundle (green) or reaction centers only (black). The samples were illuminated at 860 nm for 90 s (orange bar). The changes for samples with only reaction centers are attributable to formation and recovery of $P^+Q_A^-$. Additional changes at 453 nm and 427 nm in samples containing porphyrins are consistent with oxidation and recovery of Mn(II) $(CF_3)_2(pheF_5)_2$porphyrin and reduction and recovery of Mn(III) $(phe)_2$porphyrin, respectively

centers showed a pattern of an absorption increase at 427 nm in the light and a further increase followed by a slow decrease in the dark (Fig. 7), similar to that observed for the Mn-porphyrins bound to the MPB2 fusion reaction centers (Fig. 5). Decreasing the illumination time to 10 s or 1 s for the samples with the high-potential reaction centers resulted in the same type of behavior but with smaller amplitudes for the shorter illumination times (Fig. S45). The samples with Mn(III) $(phe)_2$porphyrin bound to the four-helix bundle showed much smaller light-induced changes at 427 nm when added to wild-type reaction centers compared to high-potential reaction centers, with very little of the absorption increase in the dark. Measurements performed on reaction centers with intermediate P^+/P midpoint potentials showed that when either Mn(III) $(phe)_2$porphyrin or Mn(III) $(mes)_2$porphyrin were bound to the four-helix bundle and added to the reaction centers, the amplitudes of the 427 nm signal increased with increasing P^+/P midpoint potentials (Fig. S44).

Discussion

The bacterial reaction center was used as a springboard to create novel electron transfer pathways involving synthetic metalloporphyrins integrated into a de novo four-helix bundle polypeptide. Optical signals of synthetic Mn-porphyrins bound to the four-helix bundle that was fused to the bacterial reaction center were consistent with reversible redox changes of the Mn-porphyrins following light absorption by the reaction centers (Figs. 4, 5). The light-induced red shift revealed oxidation of Mn(II) $(CF_3)_2(pheF_5)_2$porphyrin and Mn(II) $(CF_3)_4$porphyrin in contrast to the reverse behavior, namely a blue shift, that shows a reduction of Mn(III) $(phe)_2$porphyrin and Mn(III) $(mes)_2$porphyrin. These processes were driven by excitation of the bacteriochlorophyll dimer P and did not occur for Zn-porphyrins. The results are consistent with electron transfer between the reaction center cofactors and the Mn-porphyrins being determined by the energetics of the charge-separated states (Fig. 8). The large average difference of 0.4 V in the Mn(III)/Mn(II) midpoint potential between the fluorinated Mn(II) porphyrins and the diphenyl and dimesityl Mn(III) porphyrins sets the electron transfer into two distinct pathways, either from the Mn(II) porphyrin to the oxidized bacteriochlorophyll dimer, P^+, or from the excited state of the bacteriochlorophyll dimer, P*, to the Mn(III) porphyrin.

Consideration of the energetics indicates that the bound Mn(II) porphyrins and Mn(III) porphyrins can serve as either electron donors or acceptors, respectively. In contrast, the Zn(II) porphyrins, which lack redox transitions within the range of the reaction center cofactors, cannot

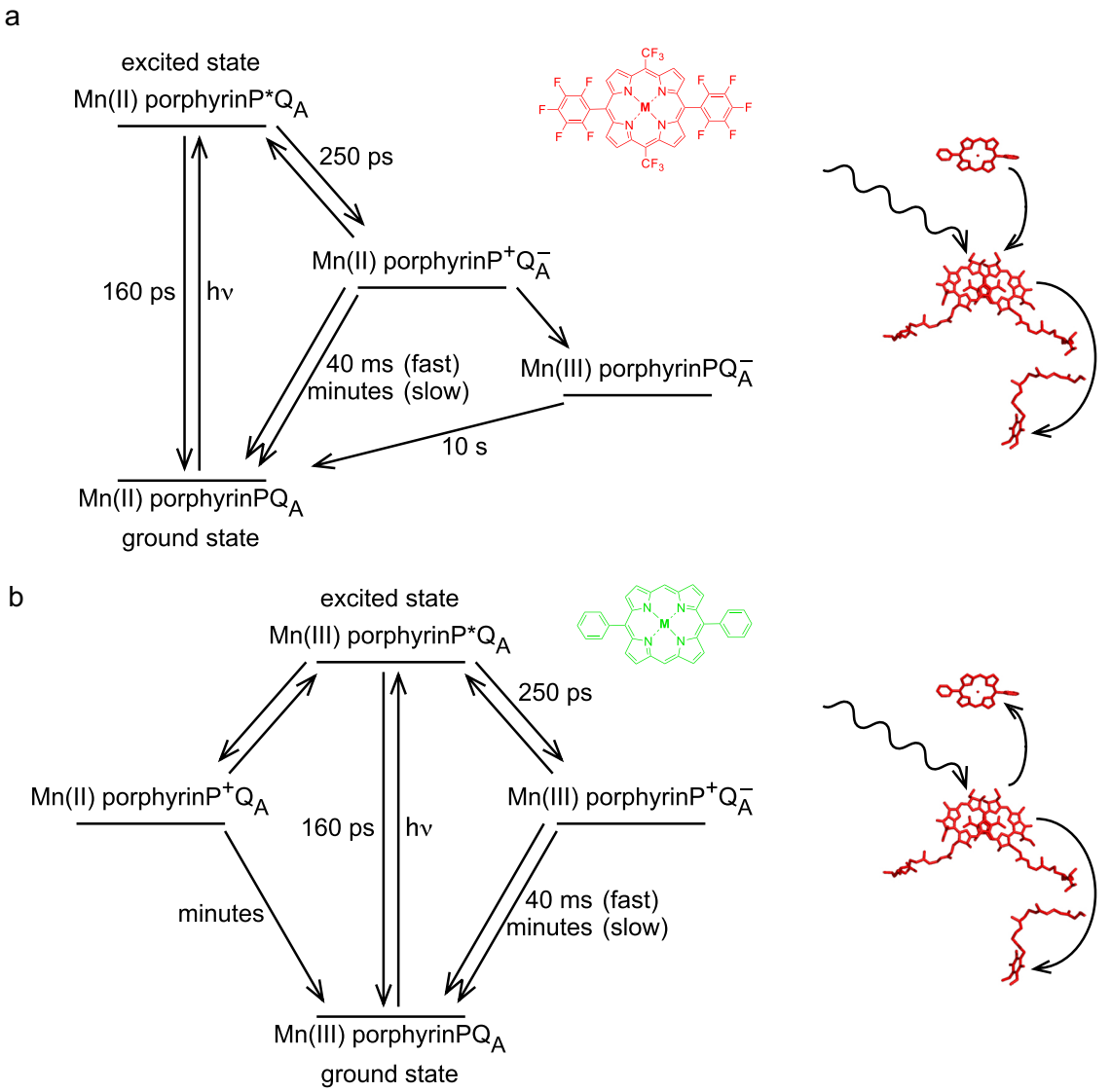

Fig. 8 Energy scheme for proposed pathways of light-induced electron transfer (curved arrows) for the hybrid reaction center with a Mn-porphyrin bound to a fused four-helix bundle, showing oxidation and reduction of two different Mn-porphyrins. In both cases, light produces the excited state, with the P/P* transition at 865 nm corresponding to the excited state being 1.43 eV above the ground state, followed by electron transfer to the primary quinone Q_A, producing the $P^+Q_A^-$ charge-separated state. In highly oxidizing reaction centers, the formation of $P^+Q_A^-$ occurs in 250 ps and $P^+Q_A^-$ recombines in 40 ms (Woodbury et al. 1995). Under continuous illumination, $P^+Q_A^-$ charge recombination also takes place on a time scale of minutes. **a** For the Mn(II) $(CF_3)_2(pheF_5)_2$porphyrin, after formation of the $P^+Q_A^-$ state, electron transfer from the Mn(II) porphyrin would result in the Mn(III) porphyrinPQ_A^- charge-separated state. This state was observed to recombine to the ground state in ~ 10 s. **b** For the Mn(III) $(phe)_2$porphyrin, electron transfer from the excited state to the Mn(III) porphyrin would generate the Mn(II) porphyrinP^+Q_A charge-separated state. The ground state was observed to recover over several minutes

participate in such electron-transfer reactions. The observation of both oxidation and reduction of the Mn-porphyrins suggests that the Mn-porphyrins are positioned at a distance suitable for electron transfer, with the direction being primarily determined by the redox properties. Because the potentials of porphyrin cofactors depend on the protein environment, binding to the four-helix bundle may shift the energies. For example, alteration of the exterior charges among the four helices results in shifts of approximately 100 mV in heme potentials (Farid et al. 2013). However, the differences in the potentials are likely to be retained. Similarly, the P^+/P midpoint potential in the MPB2 reaction centers is assumed to be close to that of the high-potential LH(L131) + LH(M160) + FH(M197) reaction center with no four-helix bundle domain. The relative differences in the midpoint potential values of the cofactors inform our

interpretation of the results for the hybrid fusion reaction centers with bound Mn-porphyrins.

The extent of the reversible redox change of all four Mn-porphyrins was dependent on the P^+/P midpoint potential, which is correlated with the rates of the electron transfer steps that involve P^+ (Fig. 7). The energy levels of the charge-separated states of the reaction center are related to the P^+/P midpoint potential, which can be changed over a range of ~ 0.3 V by mutations of the reaction center (Lin et al. 1994a). In the high-potential LH(L131) + LH(M160) + FH(M197) reaction centers, where the P^+/P midpoint potential is increased by 0.26 V compared to the wild-type value of 0.5 V, the free energy difference for the initial charge separation from P* to the bacteriopheophytin H_A is decreased, while that for charge recombination is increased, with correlated changes in the electron transfer rates (Williams and Allen 2009). For wild-type reaction centers, the formation of P* is followed by electron transfer to the bacteriopheophytin H_A in 3 ps and then to the primary quinone Q_A in 200 ps, forming the charge-separated state $P^+Q_A^-$ (Woodbury and Allen 1995; Niedringhaus et al. 2018). As a result of the increase in the P^+/P potential in the high-potential reaction centers, the time constant for electron transfer to H_A increases to 50 ps, so the total time for electron transfer from P* to $P^+Q_A^-$ is 250 ps (Woodbury et al. 1995). In wild type, the forward electron transfer time constant of 3 ps compared to the time constant for recovery to the ground state of ~ 160 ps gives a near unity value for the quantum efficiency. In the high-potential reaction centers, the slower forward electron transfer rate is closer to that of the decay of P* back to the ground state, resulting in a yield of ~ 50%. Charge recombination from the $P^+Q_A^-$ state occurs in 100 ms in wild type and in 40 ms in the high-potential reaction centers, respectively.

Oxidation of Mn(II) porphyrins

In the presence of bound Mn(II) $(CF_3)_2(pheF_5)_2$porphyrin or Mn(II) $(CF_3)_4$porphyrin, the optical changes reveal a new electron transfer step that mimics features of the reduction of P^+ by cytochrome c_2. In *R. sphaeroides*, the water-soluble cytochrome reduces P^+ after binding to the reaction center. In the fusion reaction centers, the Mn-porphyrins bind to the four-helix bundle domain at the extended C-terminus of the M subunit. Modeling places the bundle on the periplasmic surface of the reaction center with the helices perpendicular to the two-fold symmetry axis (Espiritu et al. 2017). The Mn-porphyrin would then be in a similar location as the heme of cytochrome c_2 and would have a comparable distance to the bacteriochlorophyll dimer. The Mn(III)/Mn(II) $(CF_3)_2(pheF_5)_2$porphyrin and Mn(III)/Mn(II) $(CF_3)_4$porphyrin redox potentials of 0.33 and 0.29 V vs. SHE, respectively, are close to the 0.35 V midpoint potential for cytochrome c_2, resulting in similar free energy differences for electron transfer, assuming comparable values for the potentials of the Mn-porphyrins when bound to the protein (Lin et al. 1994b). The free energy difference would increase as the P^+/P potential increases, in agreement with the observation that the extent of Mn(II) porphyrin oxidation is dependent upon the P^+/P potential (Fig. 7). Thus, consideration of the distances and energetics supports the ability of the bound Mn(II) porphyrins to donate an electron to reduce P^+ (Fig. 8A).

The comparable kinetics at the wavelengths associated with the oxidized Mn-porphyrin and reduced quinone in the light and dark are consistent with the formation and decay of the charge-separated state Mn(III) porphyrinQ_A^- (Fig. 6). The time of electron transfer from the Mn(II) porphyrin to P^+ likely occurs on a microsecond to millisecond time scale, although this rate could not be measured by the continuous light irradiation experiments reported here. In comparison, the rate of electron transfer from the heme of cytochrome c_2 to P^+ takes place in approximately 1 and 0.1 µs in wild type and the highly oxidizing reaction centers, respectively (Lin et al. 1994b). The time for Mn(II) porphyrin oxidation must be faster than the competing $P^+Q_A^-$ charge recombination time of 40 ms in order for the signal to be observed. The observed formation of the Mn(III) porphyrinQ_A^- state in a few seconds upon illumination reflects the accumulation of this state after fast continuous generation of the $P^+Q_A^-$ state balanced with the 10 s time for charge recombination from the Mn(III) porphyrinQ_A^- state. This slower charge recombination relative to $P^+Q_A^-$ charge recombination probably reflects the longer distance between the porphyrin and the quinone compared to the bacteriochlorophyll dimer and the quinone.

Reduction of Mn(III) porphyrins

For Mn(III) $(phe)_2$porphyrin and Mn(III) $(mes)_2$porphyrin, excitation of the hybrid reaction center by light results in a reduction of the Mn-porphyrins. The redox potentials of these Mn-porphyrins in solution are much lower than the redox potentials of the fluorinated Mn-porphyrins, and the difference between the types of porphyrins is assumed to be retained when bound to the protein. In this case, the Mn(III)/Mn(II) $(phe)_2$porphyrin and Mn(III)/Mn(II) $(mes)_2$porphyrin midpoint potentials in solution were − 0.05 and − 0.09 V vs. SHE, respectively. These values are very similar to the Q_A/Q_A^- midpoint potential, which has been measured to be − 0.05 V vs. SHE, with a $P/P^+Q_A^-$ free energy difference of − 0.52 eV (Dutton et al. 1973; Kleinfeld et al. 1985; Allen et al. 1998). Thus, the P^+Mn(II) porphyrin charge-separated state resulting from reduction of the Mn-porphyrin would have an energy level comparable to that found for the $P^+Q_A^-$ charge-separated state (Fig. 8B).

The spectroscopic measurements show a light-driven reduction of the bound Mn(III) porphyrins in a fully reversible process. The stability of the charge-separated states over several minutes would allow these states to build up during prolonged light exposure even if the yield from any given excitation is low. An unusual aspect of the kinetics is the continued reduction in the dark for a short period before decaying. These results can be explained with a scheme in which electron transfer occurs from P*, the excited state of the dimer, to the Mn(III) porphyrin, with the delayed dark reduction being due to repopulation of the excited state from a long-lived $P^+Q_A^-$ charge-separated state (Fig. 5). This route is hampered by the energetic barrier to repopulation of the excited state and the competition with existing pathways from the excited state. The electron transfer could proceed from P* or the intermediate charge-separated state involving the bacteriopheophytin cofactor ($P^+H_A^-$), as the energetic arguments are similar (vide infra). An alternative model for the reduction of the Mn(III) porphyrin would be by direct electron transfer from Q_A^- to the Mn(III) porphyrin. After light excitation, the reduction of the porphyrin would continue as long as Q_A^- remained. However, this reaction would have both a small free energy difference and a long distance. The Mn-porphyrin and the quinone are well buried within the protein, resulting in a much longer pathway for electron transfer from Q_A^- to the Mn(III) porphyrin than the route from P* to the Mn(III) porphyrin bound to the four-helix bundle on the donor side of the reaction center. In either the direct or indirect process, reduced Mn-porphyrin accumulates because of the prolonged presence of the $P^+Q_A^-$ state, which is due to continuous illumination and slow $P^+Q_A^-$ charge recombination. A number of experiments have identified $P^+Q_A^-$ charge recombination occurring in a multi-exponential process after continuous light exposure (van Mourik et al. 2001; Andréasson and Andréasson 2003; Manzo et al. 2011; Malferrari et al. 2013; Serdenko et al. 2016). The accumulation of the long-lived states gave rise to the idea of dark-adapted and light-adapted reaction center conformations that are proposed to be related to the protonation of amino acid residues near P (Kálmán and Maróti 1997; Deshmukh et al. 2011a, b; Allen et al. 2022).

The repopulation of the P* state has long been observed by delayed fluorescence, which refers to light emitted for a short time after exposure to an excitation light. Delayed fluorescence results from the continued presence of a population of the excited state through equilibrium with a charge-separated state (e.g., Dau and Sauer 1996). This phenomenon occurs in reaction centers from photosystem II (reviewed in Goltsev et al. 2009) and from purple bacteria (Arata and Parson 1981; Woodbury et al. 1986; McPherson et al. 1990; Turzó et al. 2000). In general, the lifetime of the delayed fluorescence in reaction centers corresponds to the lifetime of the charge-separated state, and so the observation of a continued reduction of Mn(III) $(phe)_2$porphyrin and Mn(III) $(mes)_2$porphyrin for a few minutes after illumination would be reflective of continued P* generation from reaction centers that exhibit a very slow rate of recombination from the $P^+Q_A^-$ charge-separated state. Time-resolved fluorescence measurements show that the delayed fluorescence in bacterial reaction centers is dependent on the free energy difference between the excited state and the charge-separated states, with the extent of delayed fluorescence being increased in reaction centers with high midpoint potentials (Taguchi et al. 1992; Williams et al. 1992; Peloquin et al. 1994; Woodbury et al. 1995; Onidas et al. 2013). However, the large free energy difference limits the population of P* and hence the amount of reduced Mn-porphyrin, which would depend upon the balance between the various electron transfer rates. The competing forward electron transfer and decay pathways have electron transfer time constants on the order of 100 ps, so by assuming that at least 0.1% of the time, the electron goes to the Mn-porphyrin, a limit of 0.1 µs can be estimated for the time constant for electron transfer to the Mn-porphyrin. This case illustrates the complexity of deciphering electron transfer involving multiple electron acceptors.

Conclusions

Although defining the factors required for the control of electron transfer in biological systems is a formidable challenge, the ability to create new reactions and direct them toward specific ends would advance the design of artificial proteins capable of efficient redox and associated proton-coupled electron-transfer processes. The fusion of a de novo protein containing redox-active synthetic porphyrins to bacterial reaction centers presents a singular opportunity to probe electron transfer by a strategy not available from examination of the de novo proteins or synthetic porphyrins alone. By using reaction centers as a base, redox reactions involving the synthetic porphyrins can be triggered using light excitation of the bacteriochlorophyll dimer. The versatility of this platform provides a new direction for the design of hybrid complexes to probe proton-coupled electron transfer and achieve hybrid artificial photosynthetic constructs able to drive novel redox reactions for energy production.

Supplementary Information The online version contains supplementary material available at https://doi.org/10.1007/s11120-023-01051-9.

Acknowledgements This work was supported by the U. S. Department of Energy, Office of Science, Office of Basic Energy Sciences, under Award DE-FG02-03ER15393 (A.L.M. & T.A.M.) and by the National Science Foundation CHE-1904860 (J.C.W. & J.P.A.)

Author contributions JCW, MSF, EJG, RED, KK, DAH, TAM, ALM, and JPA designed and performed research, analyzed data, and wrote the paper.

Data Availability Data available upon request.

Declarations

Competing interest The authors declare no conflict of interest.

References

Allen JP, Williams JC, Graige MS, Paddock ML, Labahn A, Feher G, Okamura MY (1998) Free energy dependence of the direct charge recombination from the primary and secondary quinones in reaction centers from *Rhodobacter sphaeroides*. Photosyn Res 55:227–233. https://doi.org/10.1023/A:1005977901937

Allen JP, Chamberlain KD, Olson TL, Williams JC (2022) A bound iron porphyrin is redox active in hybrid bacterial reaction centers modified to possess a four-helix bundle domain. Photochem Photobiol Sci 21:91–99. https://doi.org/10.1007/s43630-021-00142-7

Andréasson U, Andréasson LE (2003) Characterization of a semi-stable, charge-separated state in reaction centers from *Rhodobacter sphaeroides*. Photosynth Res 75:223–233. https://doi.org/10.1023/A:1023944605460

Arata H, Parson WW (1981) Delayed fluorescence from *Rhodopseudomonas sphaeroides* reaction centers. Enthalpy and free energy changes accompanying electron transfer from *P*-870 to quinones. Biochim Biophys Acta 638:201–209. https://doi.org/10.1016/0005-2728(81)90228-0

Arsenault EA, Guerra WD, Shee J, Reyes Cruz EA, Yoneda Y, Wadsworth BL, Odella E, Urrutia MN, Kodis G, Moore GF, Head-Gordon M, Moore AL, Moore TA, Fleming GR (2022) Concerted electron-nuclear motion in proton-coupled electron transfer-driven Grotthuss-type proton translocation. J Phys Chem Lett 13:4479–4485. https://doi.org/10.1021/acs.jpclett.2c00585

Calhoun JR, Kono H, Lahr S, Wang W, DeGrado WF, Saven JG (2003) Computational design and characterization of a monomeric helical dinuclear metalloprotein. J Mol Biol 334:1101–1115. https://doi.org/10.1016/j.jmb.2003.10.004

Chizhova NV, Maltceva OV, Zvezdina SV, Mamardashvili NZ, Koifman OI (2018) Synthesis and properties of zinc(II), cadmium(II), manganese(III), and tin(IV) octakis(4-methoxyphenyl)porphyrins. Russ J Gen Chem 88:978–984. https://doi.org/10.1134/S1070363218050249

Dau H, Sauer K (1996) Exciton equilibration and photosystem II exciton dynamics—a fluorescence study on photosystem II membrane particles of spinach. Biochim Biophys Acta 1273:175–190. https://doi.org/10.1016/0005-2728(95)00141-7

Deshmukh SS, Williams JC, Allen JP, Kálmán L (2011a) Light-induced conformational changes in photosynthetic reaction centers: dielectric relaxation in the vicinity of the dimer. Biochemistry 50:340–348. https://doi.org/10.1021/bi101496c

Deshmukh SS, Williams JC, Allen JP, Kálmán L (2011b) Light-induced conformational changes in photosynthetic reaction centers: redox-regulated proton pathway near the dimer. Biochemistry 50:3321–3331. https://doi.org/10.1021/bi200169y

Dutton PL, Leigh JS, Wraight CA (1973) Direct measurement of the midpoint potential of the primary electron acceptor in *Rhodopseudomonas spheroides* in situ and in the isolated state: some relationships with pH and *o*-phenanthroline. FEBS Lett 36:169–173. https://doi.org/10.1016/0014-5793(73)80361-8

Ennist NM, Zhao Z, Stayrook SE, Discher BM, Dutton PL, Moser CC (2022) De novo protein design of photochemical reaction centers. Nat Commun 13:4937. https://doi.org/10.1038/s41467-022-32710-5

Espiritu E, Chamberlain KD, Williams JC, Allen JP (2020) Bound manganese oxides capable of reducing the bacteriochlorophyll dimer of modified reaction centers from *Rhodobacter sphaeroides*. Photosynth Res 143:129–141. https://doi.org/10.1007/s11120-019-00680-3

Espiritu E, Olson TL, Williams JC, Allen JP (2017) Binding and energetics of electron transfer between an artificial four-helix Mn-protein and reaction centers from *Rhodobacter sphaeroides*. Biochemistry 56:6460–6469. https://doi.org/10.1021/acs.biochem.7b00978

Farid TA, Kodali G, Solomon LA, Lichtenstein BR, Sheehan MM, Fry BA, Bialas C, Ennist NM, Siedlecki JA, Zhao Z, Stetz MA, Valentine KG, Anderson JLR, Wand AJ, Discher BM, Moser CC, Dutton PL (2013) Elementary tetrahelical protein design for diverse oxidoreductase functions. Nat Chem Biol 9:826–833. https://doi.org/10.1038/nchembio.1362

Goltsev V, Zaharieva I, Chernev P, Strasser RJ (2009) Delayed fluorescence in photosynthesis. Photosynth Res 101:217–232. https://doi.org/10.1007/s11120-009-9451-1

Grayson KJ, Faries KM, Huang X, Qian P, Dilbeck P, Martin EC, Hitchcock A, Vasilev C, Yuen JM, Niedzwiedzki DM, Leggett GJ, Holten D, Kirmaier C, Hunter CN (2017) Augmenting light coverage for photosynthesis through YFP-enhanced charge separation at the *Rhodobacter sphaeroides* reaction centre. Nat Commun 8:13972. https://doi.org/10.1038/ncomms13972

Harriman A, Porter G (1979) Photochemistry of manganese porphyrins Part 1—Characterisation of some water soluble complexes. J Chem Soc Faraday Trans 2(75):1532–1542. https://doi.org/10.1039/F29797501532

Kálmán L, Maróti P (1997) Conformation-activated protonation in reaction centers of the photosynthetic bacterium *Rhodobacter sphaeroides*. Biochemistry 36:15269–15276. https://doi.org/10.1021/bi971882q

Kleinfeld D, Okamura MY, Feher G (1985) Electron transfer in reaction centers of *Rhodopseudomonas sphaeroides*. II. Free energy and kinetic relations between the acceptor states $Q_A^- Q_B^-$ and $Q_A Q_B^{2-}$. Biochim Biophys Acta 809:291–310. https://doi.org/10.1016/0005-2728(85)90179-3

Lin C, Fang MY, Cheng SH (2002) Substituent and axial ligand effects on the electrochemistry of zinc porphyrins. J Electroanal Chem 531:155–162. https://doi.org/10.1016/S0022-0728(02)01056-2

Lin X, Murchison HA, Nagarajan V, Parson WW, Allen JP, Williams JC (1994a) Specific alteration of the oxidation potential of the electron donor in reaction centers from *Rhodobacter sphaeroides*. Proc Natl Acad Sci USA 91:10265–10269. https://doi.org/10.1073/pnas.91.22.10265

Lin X, Williams JC, Allen JP, Mathis P (1994b) Relationship between rate and free energy difference for electron transfer from cytochrome c_2 to the reaction center in *Rhodobacter sphaeroides*. Biochemistry 33:13517–13523. https://doi.org/10.1021/bi00250a002

Liu J, Friebe VM, Frese RN, Jones MR (2020) Polychromatic solar energy conversion in pigment-protein chimeras that unite the two kingdoms of (bacterio)chlorophyll-based photosynthesis. Nat Commun 11:1542. https://doi.org/10.1038/s41467-020-15321-w

Lombardi A, Pirro F, Maglio O, Chino M, DeGrado WF (2019) De novo design of four-helix bundle metalloproteins: one scaffold, diverse reactivities. Acc Chem Res 52:1148–1159. https://doi.org/10.1021/acs.accounts.8b00674

Lu P, Min D, DiMaio F, Wei KY, Vahey MD, Boyken SE, Chen Z, Fallas JA, Ueda G, Sheffler W, Mulligan VK, Xu W, Bowie JU, Baker D (2018) Accurate computational design of multipass transmembrane proteins. Science 359:1042–1046. https://doi.org/10.1126/science.aaq1739

Malferrari M, Mezzetti A, Francia F, Venturoli G (2013) Effects of dehydration on light-induced conformational changes in bacterial photosynthetic reaction centers probed by optical and differential

FTIR spectroscopy. Biochim Biophys Acta 1827:328–339. https://doi.org/10.1016/j.bbabio.2012.10.009

Mancini JA, Kodali G, Jiang J, Reddy KR, Lindsey JS, Bryant DA, Dutton PL, Moser CC (2017) Multi-step excitation energy transfer engineered in genetic fusions of natural and synthetic light-harvesting proteins. J R Soc Interface 14:20160896. https://doi.org/10.1098/rsif.2016.0896

Mann SI, Nayak A, Gassner GT, Therien MJ, DeGrado WF (2021) De novo design, solution characterization, and crystallographic structure of an abiological Mn–porphyrin-binding protein capable of stabilizing a Mn(V) species. J Am Chem Soc 143:252–259. https://doi.org/10.1021/jacs.0c10136

Manzo AJ, Goushcha AO, Berezetska NM, Kharkyanen VN, Scott GW (2011) Charge recombination time distributions in photosynthetic reaction centers exposed to alternating intervals of photoexcitation and dark relaxation. J Phys Chem B 115:8534–8544. https://doi.org/10.1021/jp1115383

McPherson PH, Nagarajan V, Parson WW, Okamura MY, Feher G (1990) pH-dependence of the free energy gap between DQ_A and $D^+Q_A^-$ determined from delayed fluorescence in reaction centers from *Rhodobacter sphaeroides* R-26. Biochim Biophys Acta 1019:91–94. https://doi.org/10.1016/0005-2728(90)90128-Q

Mora SJ, Odella E, Moore GF, Gust D, Moore TA, Moore AL (2018) Proton-coupled electron transfer in artificial photosynthetic systems. Acc Chem Res 51:445–453. https://doi.org/10.1021/acs.accounts.7b00491

Niedringhaus A, Policht VR, Sechrist R, Konar A, Laible PD, Bocian DF, Holten D, Kirmaier C, Ogilvie JP (2018) Primary processes in the bacterial reaction center probed by two-dimensional electronic spectroscopy. Proc Natl Acad Sci USA 115:3563–3568. https://doi.org/10.1073/pnas.1721927115

Okamura MY, Paddock ML, Graige MS, Feher G (2000) Proton and electron transfer in bacterial reaction centers. Biochim Biophys Acta 1458:148–163. https://doi.org/10.1016/S0005-2728(00)00065-7

Olson TL, Espiritu E, Edwardraja S, Simmons CR, Williams JC, Ghirlanda G, Allen JP (2016) Design of dinuclear manganese cofactors for bacterial reaction centers. Biochim Biophys Acta 1857:539–547. https://doi.org/10.1016/j.bbabio.2015.09.003

Olson TL, Espiritu E, Edwardraja S, Canarie E, Flores M, Williams JC, Ghirlanda G, Allen JP (2017) Biochemical and spectroscopic characterization of dinuclear Mn-sites in artificial four-helix bundle proteins. Biochim Biophys Acta 1858:945–954. https://doi.org/10.1016/j.bbabio.2017.08.013

Onidas D, Sipka G, Asztalos E, Maróti P (2013) Mutational control of bioenergetics of bacterial reaction center probed by delayed fluorescence. Biochim Biophys Acta 1827:1191–1199. https://doi.org/10.1016/j.bbabio.2015.09.003

Peloquin JM, Williams JC, Lin X, Alden RG, Taguchi AKW, Allen JP, Woodbury NW (1994) Time-dependent thermodynamics during early electron transfer in reaction centers from *Rhodobacter sphaeroides*. Biochemistry 33:8089–8100. https://doi.org/10.1021/bi00192a014

Porhiel E, Bondon A, Leroy J (2000) (β-octafluoro-*meso*-tetraarylporphyrin) manganese complexes: synthesis, characterization and catalytic behaviour in monooxygenation reactions. Eur J Inorg Chem 2000:1097–1105. https://doi.org/10.1002/(SICI)1099-0682(200005)2000:5%3C1097::AID-EJIC1097%3E3.0.CO;2-2

Serdenko TV, Barabash YM, Knox PP, Seifullina NK (2016) The kinetic model for slow photoinduced electron transport in the reaction centers of purple bacteria. Nanoscale Res Lett 11:286. https://doi.org/10.1186/s11671-016-1502-x

Shimizu S, Aratani N, Osuka A (2006) meso-Trifluoromethyl-substituted expanded porphyrins. Chem Eur J 12:4909–4918. https://doi.org/10.1002/chem.200600158

Taguchi AKW, Stocker JW, Alden RG, Causgrove TP, Peloquin JM, Boxer SG, Woodbury NW (1992) Biochemical characterization and electron-transfer reactions of *sym1*, a *Rhodobacter capsulatus* reaction center symmetry mutant which affects the initial electron donor. Biochemistry 31:10345–10355. https://doi.org/10.1021/bi00157a024

Turzó K, Laczkó G, Filus Z, Maróti P (2000) Quinone-dependent delayed fluorescence from the reaction center of photosynthetic bacteria. Biophys J 79:14–25. https://doi.org/10.1016/S0006-3495(00)76270-9

van Mourik F, Reus M, Holzwarth AR (2001) Long-lived charge-separated states in bacterial reaction centers isolated from *Rhodobacter sphaeroides*. Biochim Biophys Acta 1504:311–318. https://doi.org/10.1016/S0005-2728(00)00259-0

Wijesekera TP (1996) 5-Perfluoroalkyldipyrromethanes and porphyrins derived therefrom. Can J Chem 74:1868–1871. https://doi.org/10.1139/v96-209

Williams JC, Alden RG, Murchison HA, Peloquin JM, Woodbury NW, Allen JP (1992) Effects of mutations near the bacteriochlorophylls in reaction centers from *Rhodobacter sphaeroides*. Biochemistry 31:11029–11037. https://doi.org/10.1021/bi00160a012

Williams JC, Allen JP (2009) Directed modification of reaction centers from purple bacteria. In: Hunter CN, Daldal F, Thurnauer MC, Beatty JT (eds) The purple phototrophic bacteria. Springer, Dordrecht, pp 337–353

Woodbury NW, Parson WW, Gunner MR, Prince RC, Dutton PL (1986) Radical-pair energetics and decay mechanisms in reaction centers containing anthraquinones, naphthoquinones or benzoquinones in place of ubiquinone. Biochim Biophys Acta 851:6–22. https://doi.org/10.1016/0005-2728(86)90243-4

Woodbury NW, Lin S, Lin X, Peloquin JM, Taguchi AKW, Williams JC, Allen JP (1995) The role of reaction center excited state evolution during charge separation in a *Rb. sphaeroides* mutant with an initial electron donor midpoint potential 260 mV above wild type. Chem Phys 197:405–421. https://doi.org/10.1016/0301-0104(95)00170-S

Woodbury NW, Allen JP (1995) The pathway, kinetics, and thermodynamics of electron transfer in wild type and mutant reaction centers of purple nonsulfur bacteria. In: Blankenship RE, Madigan MT, Bauer CE (eds) Anoxygenic photosynthetic bacteria. Kluwer Academic Publishers, Netherlands, pp 527–557

Wraight CA (2006) Chance and design–proton transfer in water, channels and bioenergetic proteins. Biochim Biophys Acta 1757:886–912. https://doi.org/10.1016/j.bbabio.2006.06.017

Yang C, Sesterhenn F, Bonet J, van Aalen EA, Scheller L, Abriata LA, Cramer JT, Wen X, Rosset S, Georgeon S, Jardetzky T, Krey T, Fussenegger M, Merkx M, Correia BE (2021) Bottom-up de novo design of functional proteins with complex structural features. Nat Chem Biol 17:492–500. https://doi.org/10.1038/s41589-020-00699-x

Yoneda Y, Mora SJ, Shee J, Wadsworth BL, Arsenault EA, Hait D, Kodis G, Gust D, Moore GF, Moore AL, Head-Gordon M, Moore TA, Fleming GR (2021) Electron–nuclear dynamics accompanying proton-coupled electron transfer. J Am Chem Soc 143:3104–3112. https://doi.org/10.1021/jacs.0c10626